Supplement of Atmos. Chem. Phys., 16, 9965–9981, 2016
http://www.atmos-chem-phys.net/16/9965/2016/
doi:10.5194/acp-16-9965-2016-supplement

Supplement of

High-resolution simulation of link-level vehicle emissions and concentrations for air pollutants in a traffic-populated eastern Asian city

Shaojun Zhang et al.

Correspondence to: Ye Wu (ywu@tsinghua.edu.cn)

Supplementary Tables

Table S1. Estimated traffic activity by vehicle category in Macau during a typical weekday of 2010

Vehicle category	Traffic activity (veh km d^{-1})	Vehicle category	Traffic activity (veh km d^{-1})
LDPV	1.72×10^{6}	Taxi	6.01×10^{5}
MDPV	1.08×10^{5}	Motorcycle	1.23×10^{6}
HDPV	8.44×10^{4}	LDT	1.37×10^{5}
Public bus	1.42×10^{5}	HDT	2.12×10^{4}

Table S2. Spatial allocation of vehicle emissions in Macau during a typical weekday of 2010

Region / Parish	Allocation of vehicle emissions				
	CO	THC	NO_X	$PM_{2.5}$	CO_2
Macau Peninsula	76%	78%	58%	52%	59%
St. Lazarus Parish	12%	12%	9%	8%	9%
St. Lawrence Parish	8%	8%	6%	5%	6%
Our Lady Fatima Parish	23%	25%	17%	15%	18%
St. Anthony Parish	16%	17%	12%	10%	13%
Cathedral Parish	16%	16%	14%	13%	13%
Taipa	12%	10%	21%	23%	19%
CoTai Reclamation Area	5%	5%	9%	10%	8%
Coloane	2%	2%	2%	2%	3%
Others (three cross-sea bridges)	6%	5%	10%	13%	10%

Supplementary Figures

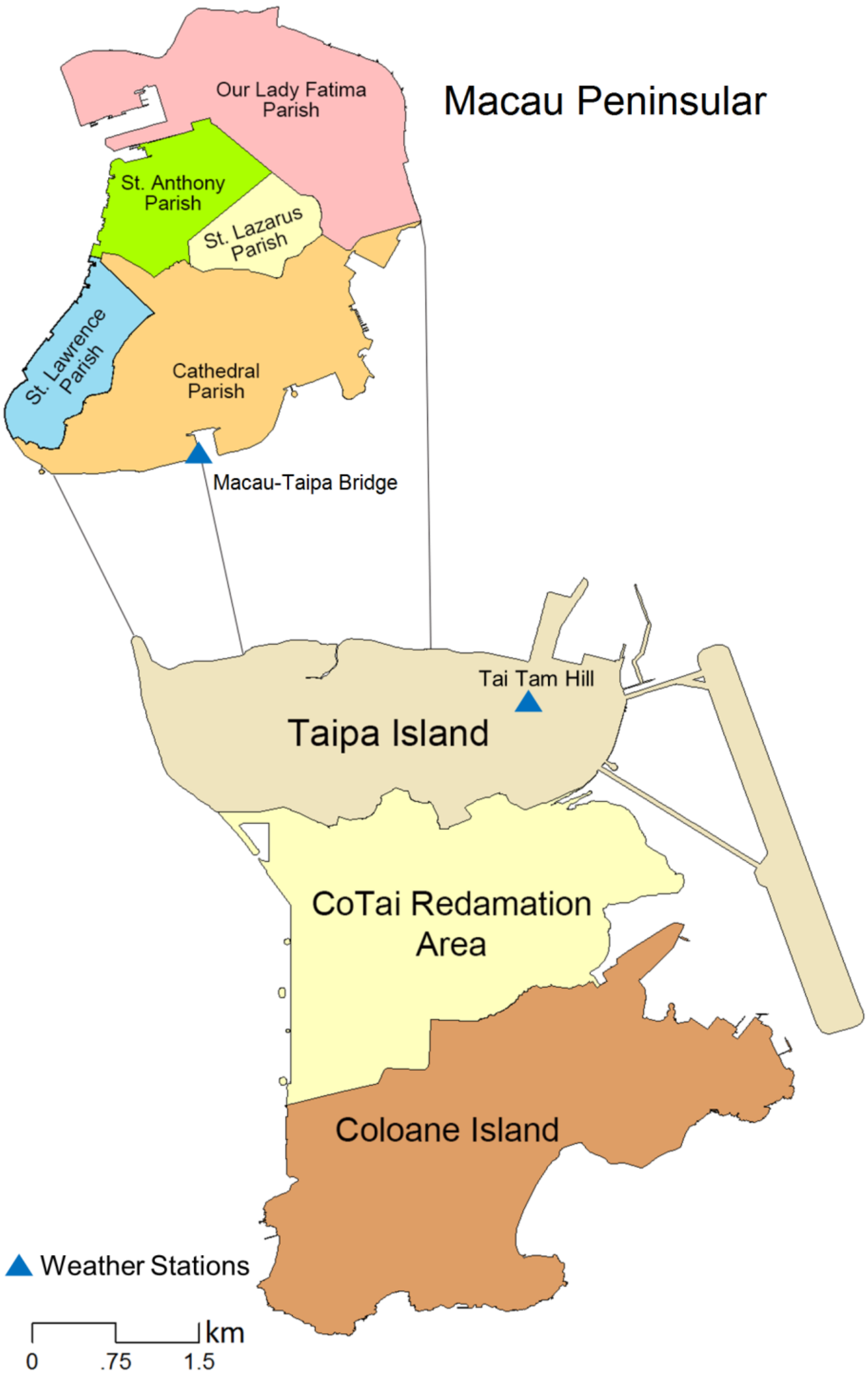

Fig. S1. Map of the Special Administrative Region of Macau, China
Two weather stations are marked in the figure.

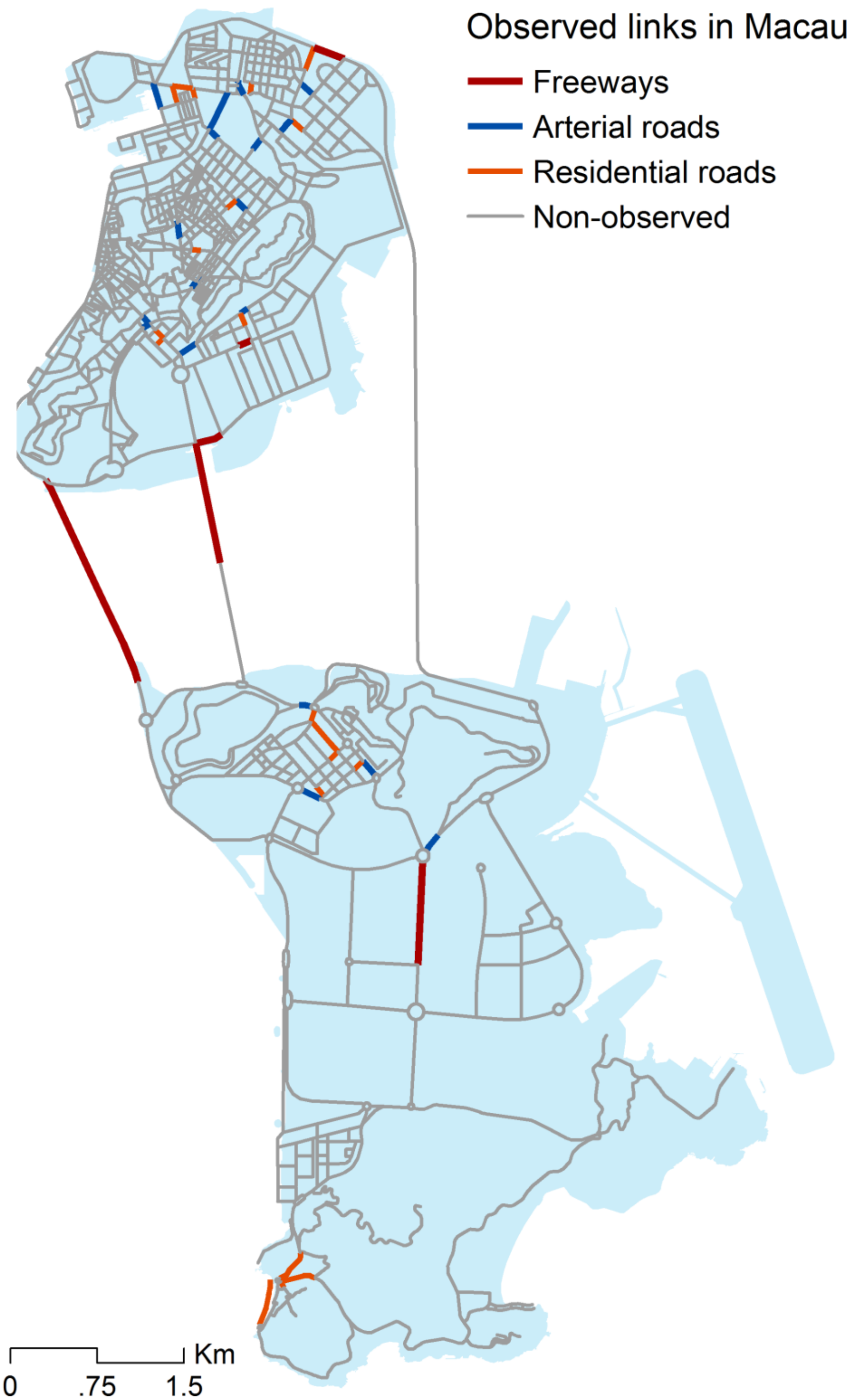

Fig. S2. Map of the road links with observed traffic volume data

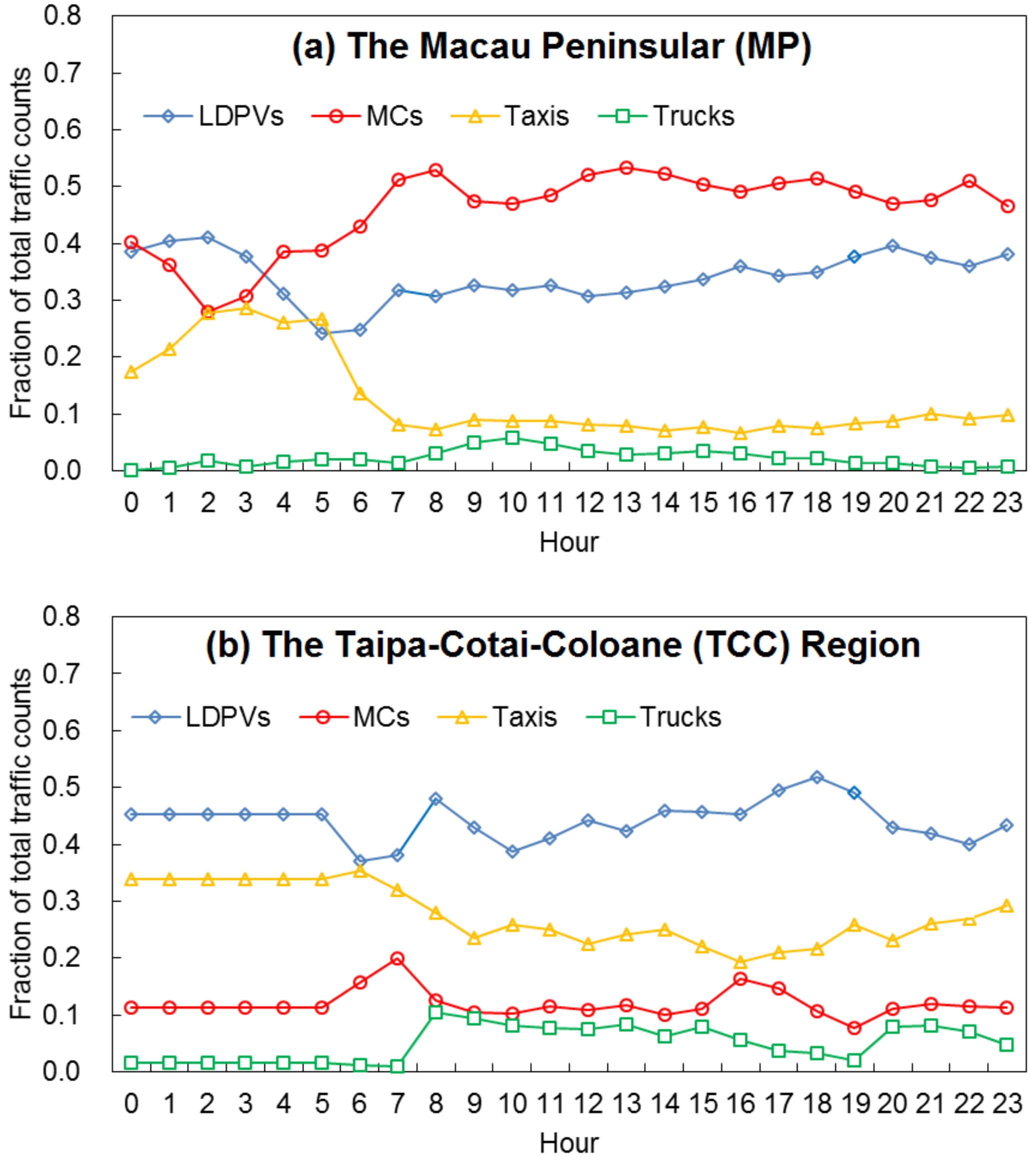

Fig. S3. Hourly allocations of traffic volume for LDPVs, motorcycles, taxis and trucks on the arterial roads in (a) the Macau Peninsula and (b) the Taipa-Cotai-Coloane Region.

Note: Hourly truck volume data in this figure is the combined results for LDTs and HDTs.

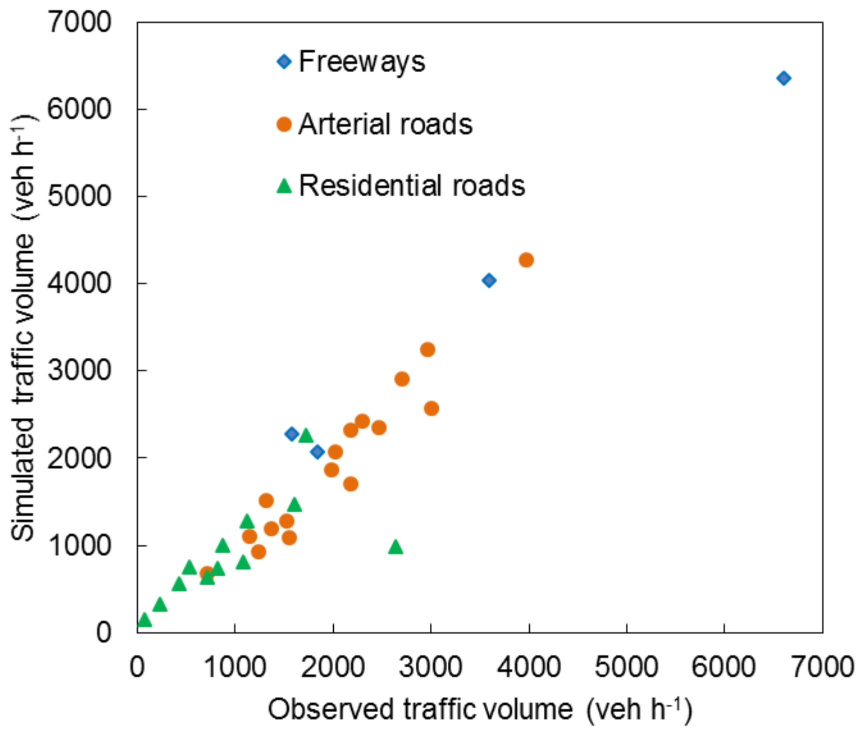

Fig. S4. Comparison of observed traffic volume and simulated results with the TransCAD model for 33 roads during 6 p.m. hour of typical weekdays

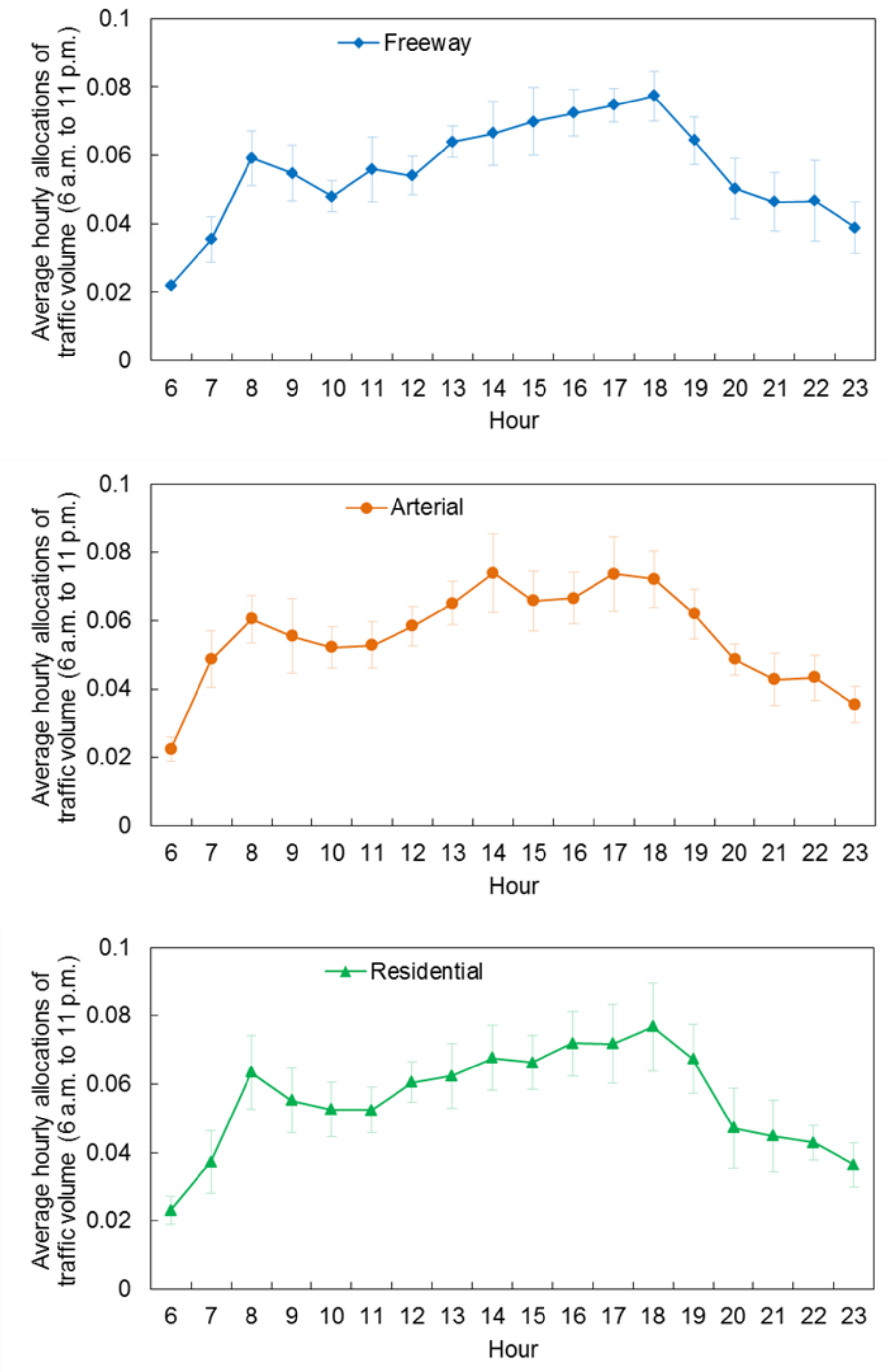

Fig. S5. Average allocations of hourly traffic volume in the total traffic volume from 6 a.m. to 11 p.m. Only roads with observed traffic volume data are included.

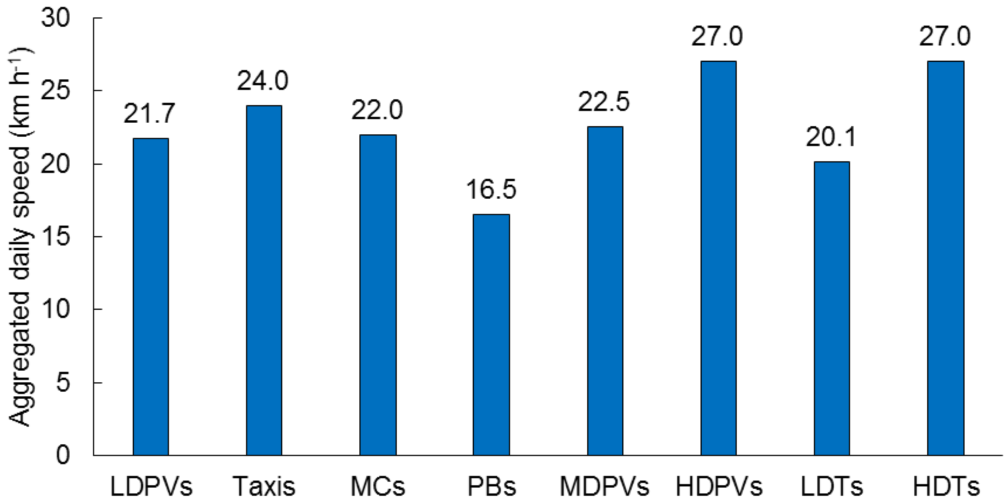

Fig. S6. Fleet-average speed of each vehicle category in Macau, during a typical weekday of 2010.

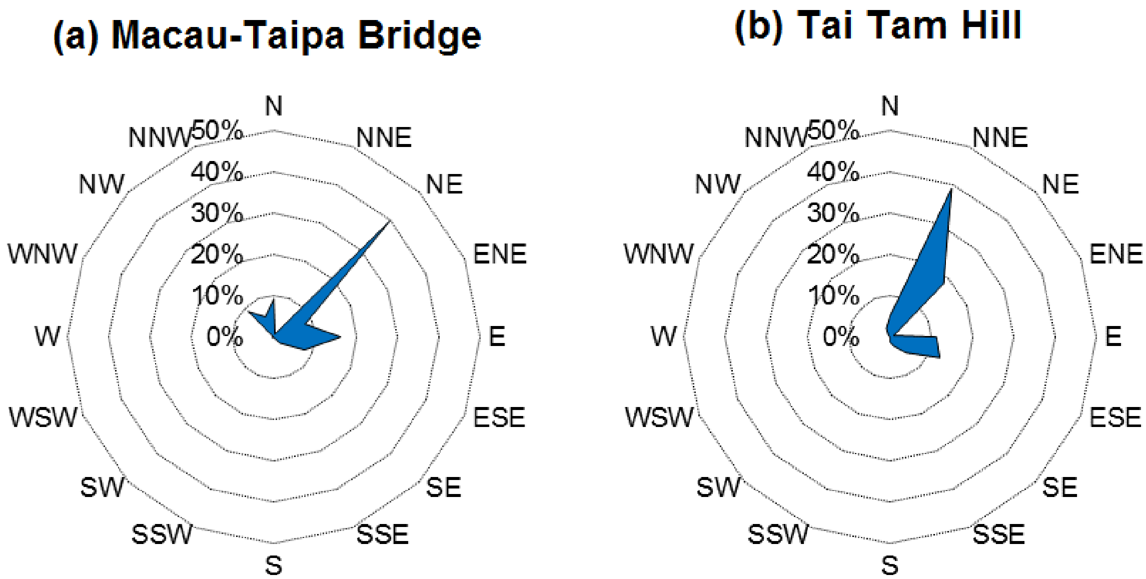

Fig. S7. Wind rose map of two weather stations in Macau during weekdays of November 2010.

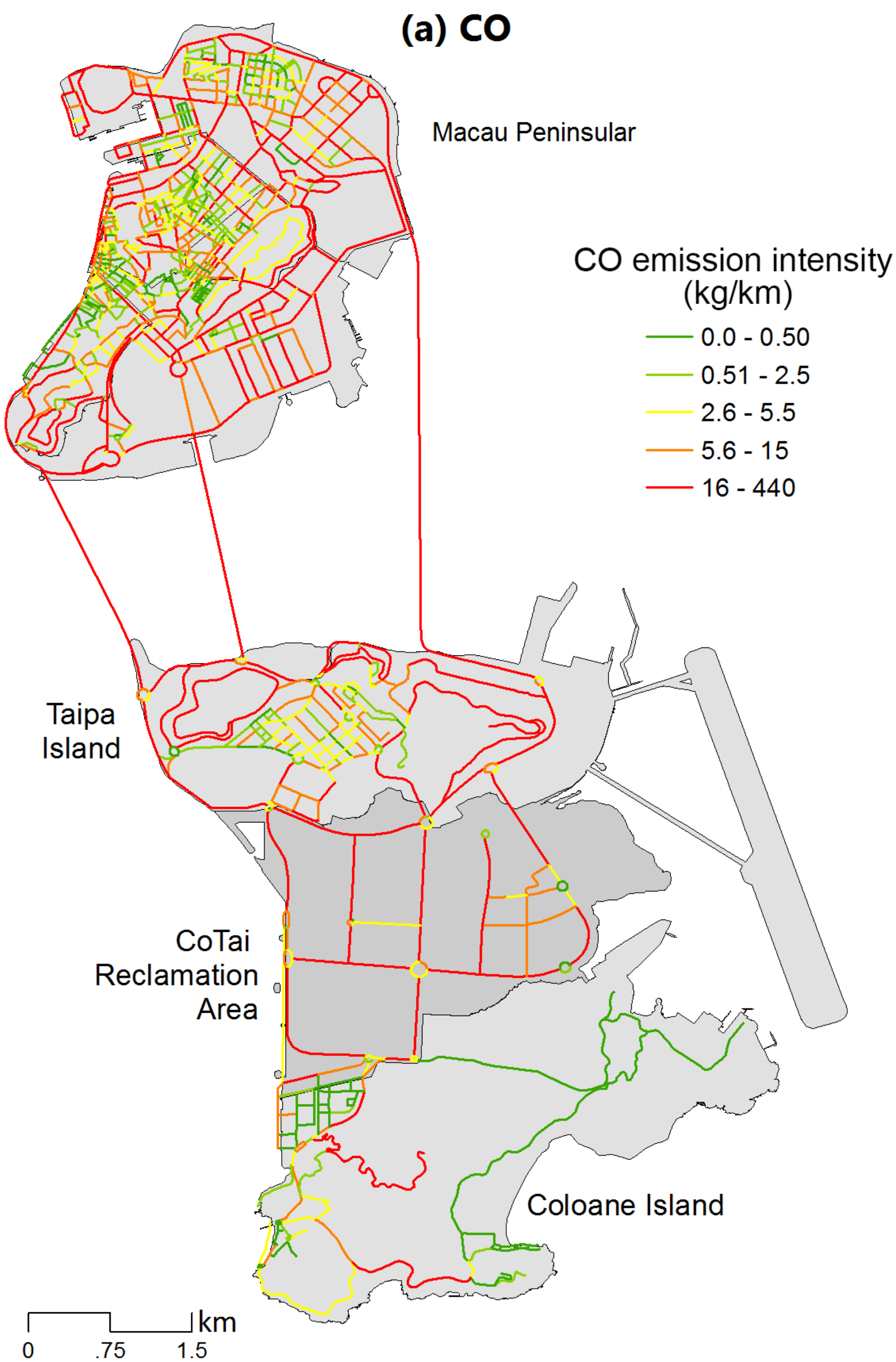

(a) CO
Macau Peninsular
CO emission intensity
(kg/km)
0.0 - 0.50
0.51 - 2.5
2.6 - 5.5
5.6 - 15
16 - 440
Taipa
Island
CoTai
Reclamation
Area
Coloane Island
km
0
.75
1.5

1

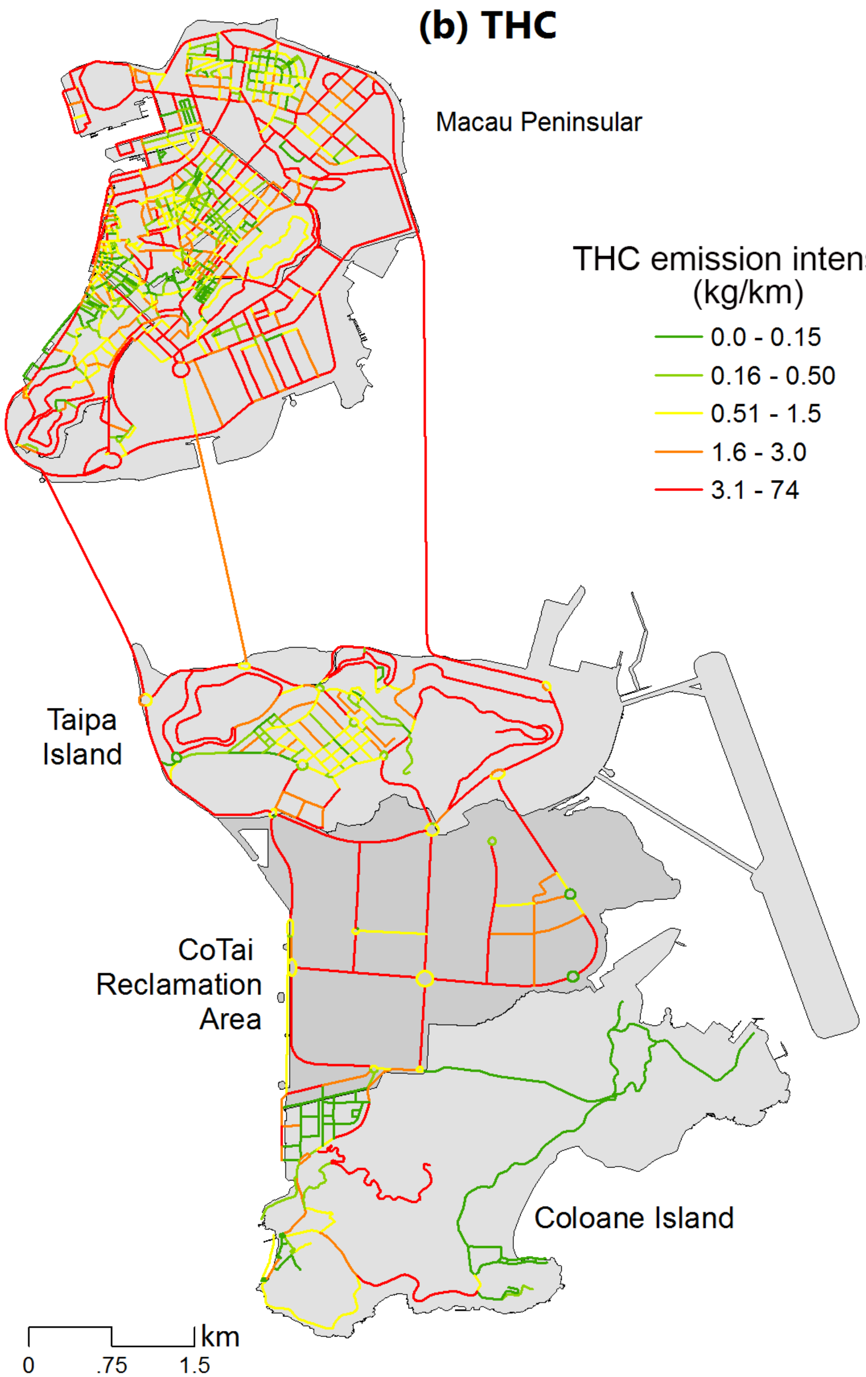

(b) THC
Macau Peninsular
THC emission intensity
(kg/km)
0.0 - 0.15
0.16 - 0.50
0.51 - 1.5
1.6 - 3.0
3.1 - 74
Taipa
Island
CoTai
Reclamation
Area
Coloane Island
km
0
.75
1.5

1

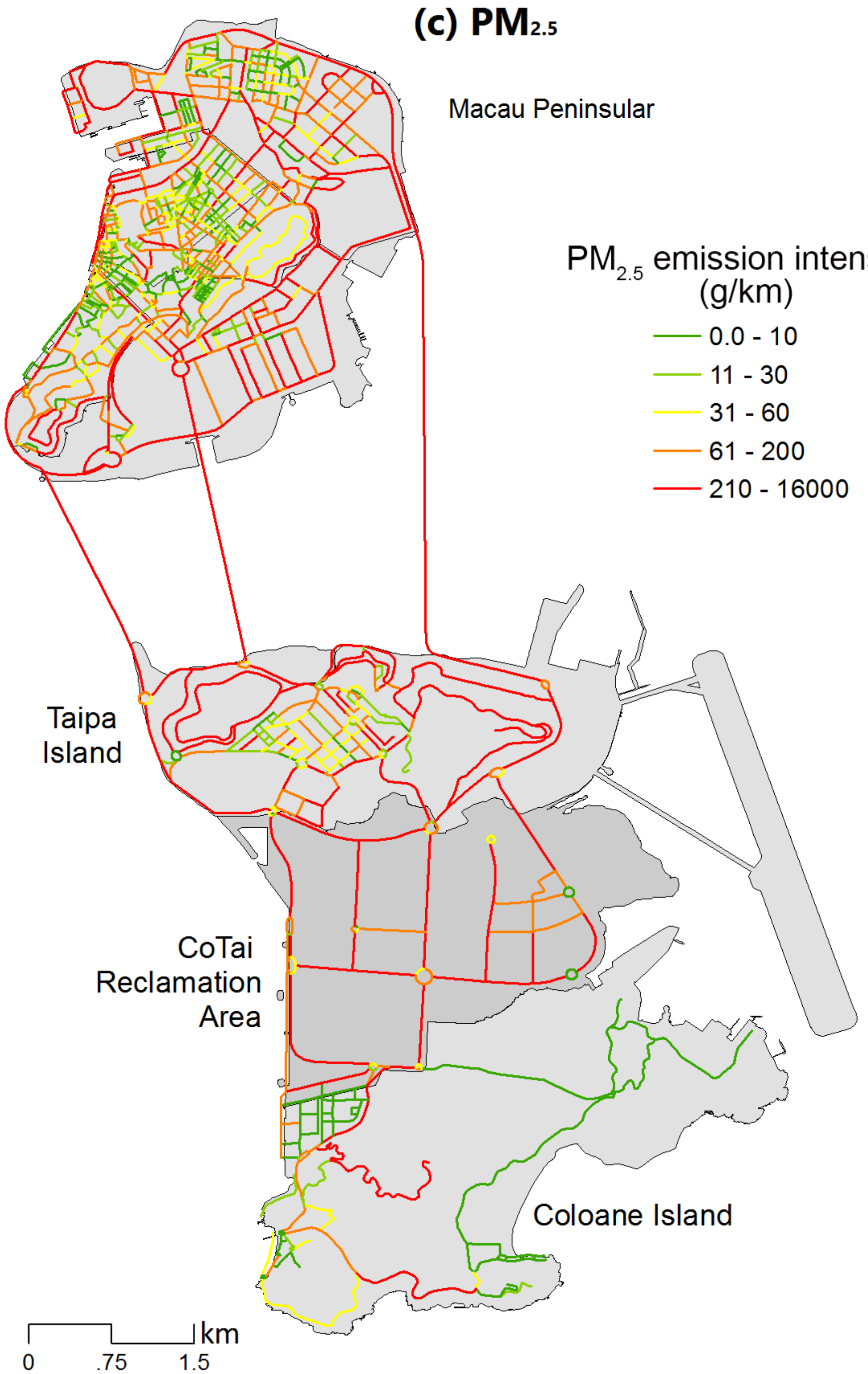

2 Fig. S8. The spatial distribution of vehicle emissions for (a) CO, (b) THC, (c) $PM_{2.5}$ and (d) CO_2 in
3 Macau during a typical weekday of 2010

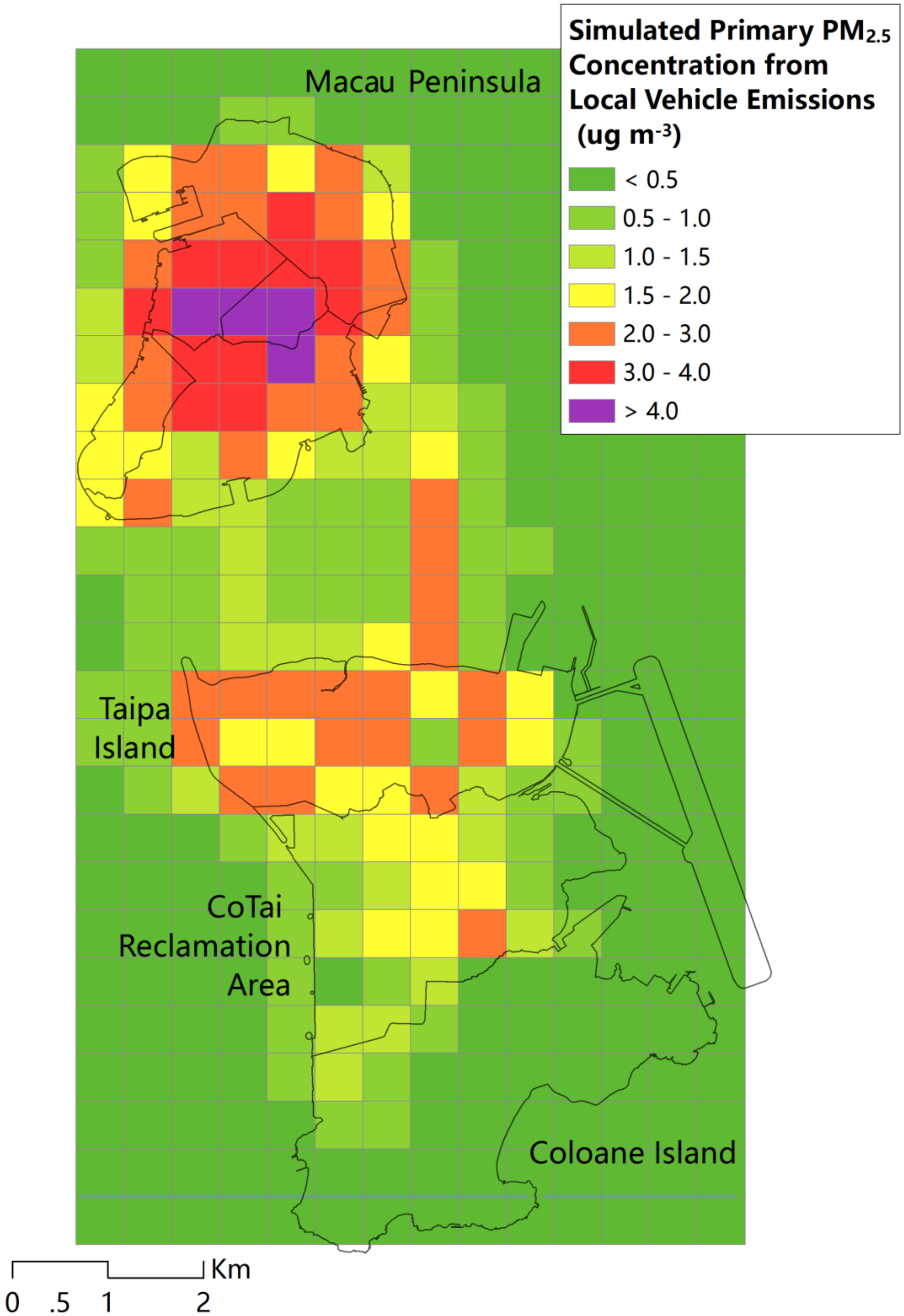

Fig. S9. Simulated vehicle-contributed concentrations of $PM_{2.5}$ in Macau during weekdays of November, 2010

Air Quality Modeling with the CMAQ model

In this study, the Weather Research Forecasting model (WRF, version 3.3) and Community Multiscale Air Quality model (CMAQ, version 4.7.1) were employed to investigate impacts from regional background, cross-boundary transport and other area sources. National Centers for Environmental Prediction (NCEP) and the automated data processing (ADP) data, with a resolution of 1°× 1° were used as initial guess fields of WRF. Four-dimensional data assimilation (FDDA) is applied for objective analysis. Detailed physical parameterizations include the Kain-Fritsch 2 cumulus scheme, the Pleim-Xiu PBL scheme and land surface model, the mixed phase explicit moisture scheme for cloud microphysics, the cloud-radiation shortwave radiation scheme and the Rapid Radiative Transfer Model (RRTM) longwave radiation scheme. The Meteorology Chemistry Interface Processor (MCIP) version 3.6 was applied to process the meteorological data to the data format for CMAQ. CB-05 gas-phase chemical mechanism with AERO5 aerosol module were used. The aerosol thermodynamic equilibrium model is ISORROPIA.

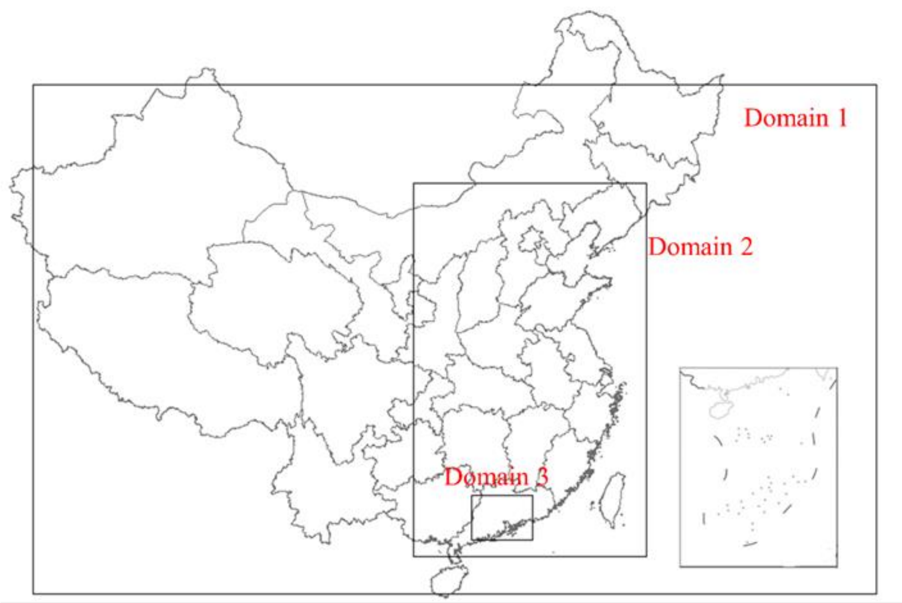

Fig. S10. Triple-nested simulation domain of CMAQ at a horizontal grid resolution of 36 km, 12 km and 4 km.

A triple-nested simulation domain, shown in Figure S10, was used in this study. Domain 1 covers most of China of 36 km × 36 km horizontal resolution. Domain 2 covers East of China with 12 km × 12 km horizontal resolution. Domain 3 covers Perl River Delta (PRD) with 4 km × 4 km horizontal resolution. 23 vertical layers (σ: 1.000、0.995、0.988、0.980、0.970、0.956、0.938、0.916、0.893、0.868、0.839、 0.808、0.777、0.744、0.702、0.648、0.582、0.500、0.400、0.300、0.200、0.120、0.052 and 0.000) were included ranging from surface to 100 mbar. The configurations of chemical initial conditions and boundary conditions, and regional emission inventory are consistent with our previous papers (Zhao et al 2013a, 2013b). The local emissions for other sectors (e.g., residential, power, and industrial sectors) in Macau were provided by the Macau Environmental Protection Bureau, together with the vehicle emissions estimated by this study. The simulated results of regional air quality are presented in Fig. S11.

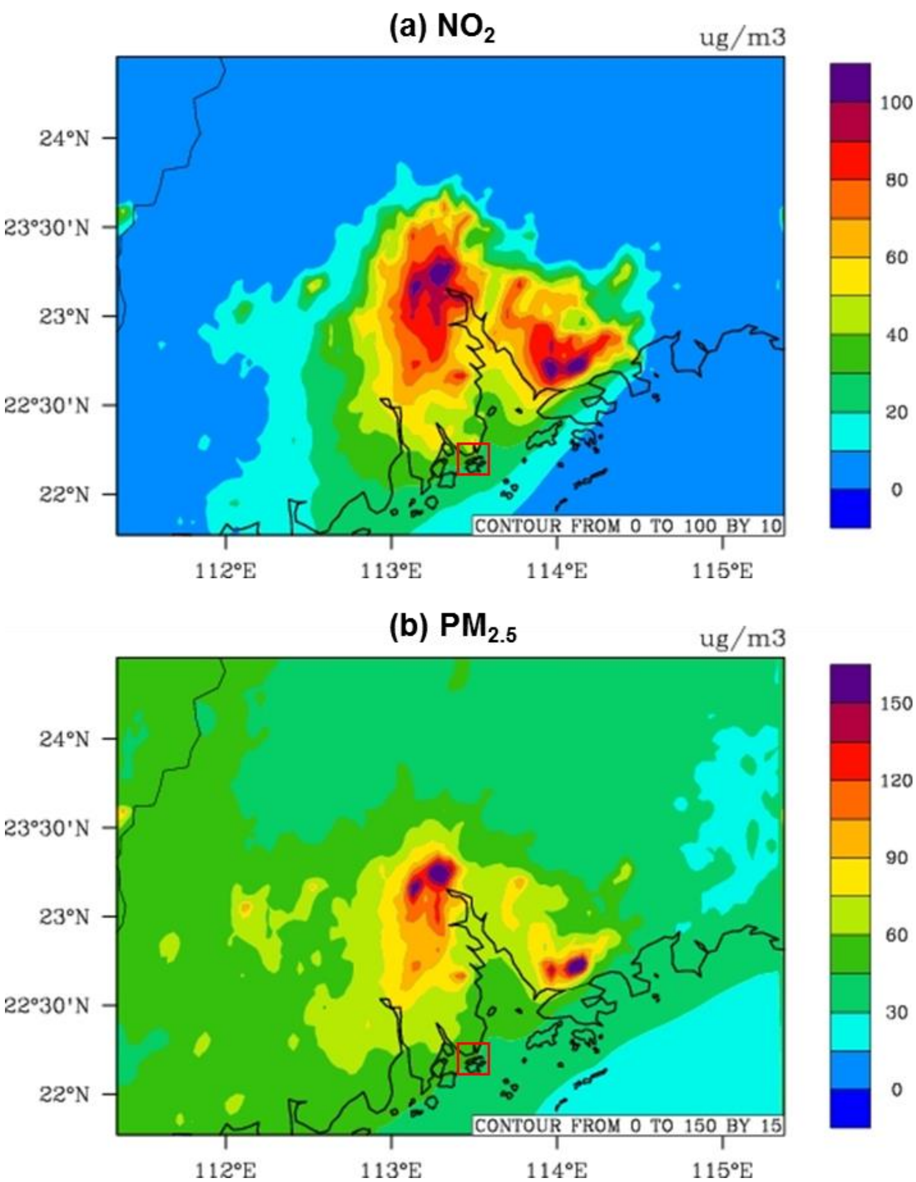

Fig. S11. Monthly average of simulated concentrations for NO_2 and $PM_{2.5}$ in the Pearl River Delta Region (i.e., Domain 3), November 2010

Simulated monthly average concentrations of NO_2 and $PM_{2.5}$ (November 2010) of the 4 km × 4 km cells are presented in Table S3, within which the air quality stations are located. We also include the observed NO_2 and PM_{10} concentrations during November 2010 for comparison. It is noted that the $PM_{2.5}$ monitoring was not conducted in Macau until July 2012. The one-year monitoring results in 2013 indicate that the mass fraction of $PM_{2.5}$ in PM_{10} was approximately 60%. The CMAQ model is not capable of the high NO_2 concentrations in Macau with normalized mean bias of -37% to 55%. On the other hand, although the AERMOD model may yield higher NO_2 concentrations in traffic populated areas, however, the model limitations would bring in considerable uncertainty (e.g., diurnal fluctuations). Thus, we suggest that future efforts are required to develop more advanced air quality model to enhance spatial heterogeneity and chemical transport at the same time.

Table S3. Comparison of simulated and observed air pollutant concentrations, monthly average of November 2010 ($\mu g\ m^{-3}$, mean ± standard deviation)

Monitoring sites	Observed NO_2	Simulated NO_2	NMB	Observed PM_{10}	Simulated $PM_{2.5}$	NMB [a]
MP 1	68.0±12.7	37.8±16.7	-44%	99.1±28.6	41.2±18.3	-31%
MP 2	64.9±13.1	40.8±14.3	-37%	96.6±30.3	41.8±17.1	-28%
Taipa 1	52.2±10.4	33.1±16.8	-37%	84.8±23.1	37.0±16.7	-27%
Taipa 2	55.1±14.8	29.3±15.9	-47%	86.5±14.8	33.2±16.6	-36%
Coloane	65.0±17.3	29.8±16.5	-54%	86.1±24.9	34.8±17.8	-33%

Note: [a] We assume that the mass fraction of $PM_{2.5}$ in PM_{10} was 0.6.

References

Zhao, B.; Wang, S. X.; Dong, X. Y.; Wang, J. D.; Duan, L.; Fu, X.; Hao, J. M.; Fu, J., Environmental effects of the recent emission changes in China: implications for particulate matter pollution and soil acidification. *Environmental Research Letters* **2013a,** *8*, (2).

Zhao, B.; Wang, S.; Wang, J.; Fu, J. S.; Liu, T.; Xu, J.; Fu, X.; Hao, J., Impact of national NOx and SO_2 control policies on particulate matter pollution in China. *Atmospheric Environment* **2013b,** *77*, (0), 453-463.